POLITECNICO DI TORINO
Repository ISTITUZIONALE

Evidence of Two Resonant Structures in e+e- +hc

Original
Evidence of Two Resonant Structures in e+e- +hc / Ablikim, M., Achasov, M.N., Ahmed, S., Ai, X.C., Albayrak, O., Albrecht, M., Ambrose, D.J., Amoroso, A., An, F.F., An, Q., Bai, J.Z., Bakina, O., Baldini Ferroli, R., Ban, Y., Bennett, D.W., Bennett, J.V., Berger, N., Bertani, M., Bettoni, D., Bian, J.M., et al.. - In: PHYSICAL REVIEW LETTERS. - ISSN 0031-9007. - 118:9(2017), p. 092002. [10.1103/PhysRevLett.118.092002]

Availability:
This version is available at: 11583/2682569 since: 2017-09-27T10:07:31Z

Publisher:
American Physical Society

Published
DOI:10.1103/PhysRevLett.118.092002

Terms of use:

This article is made available under terms and conditions as specified in the corresponding bibliographic description in the repository

Publisher copyright

(Article begins on next page)

07 October 2026

arXiv:1610.07044v2 [hep-ex] 2 Mar 2017

Evidence of Two Resonant Structures in $e^+e^- \to \pi^+\pi^- h_c$

M. Ablikim[1], M. N. Achasov[9,e], S. Ahmed[14], X. C. Ai[1], O. Albayrak[5], M. Albrecht[4], D. J. Ambrose[44], A. Amoroso[49A,49C], F. F. An[1], Q. An[46,a], J. Z. Bai[1], O. Bakina[23], R. Baldini Ferroli[20A], Y. Ban[31], D. W. Bennett[19], J. V. Bennett[5], N. Berger[22], M. Bertani[20A], D. Bettoni[21A], J. M. Bian[43], F. Bianchi[49A,49C], E. Boger[23,c], I. Boyko[23], R. A. Briere[5], H. Cai[51], X. Cai[1,a], O. Cakir[40A], A. Calcaterra[20A], G. F. Cao[1], S. A. Cetin[40B], J. Chai[49C], J. F. Chang[1,a], G. Chelkov[23,c,d], G. Chen[1], H. S. Chen[1], J. C. Chen[1], M. L. Chen[1,a], S. Chen[41], S. J. Chen[29], X. Chen[1,a], X. R. Chen[26], Y. B. Chen[1,a], X. K. Chu[31], G. Cibinetto[21A], H. L. Dai[1,a], J. P. Dai[34], A. Dbeyssi[14], D. Dedovich[23], Z. Y. Deng[1], A. Denig[22], I. Denysenko[23], M. Destefanis[49A,49C], F. De Mori[49A,49C], Y. Ding[27], C. Dong[30], J. Dong[1,a], L. Y. Dong[1], M. Y. Dong[1,a], Z. L. Dou[29], S. X. Du[53], P. F. Duan[1], J. Z. Fan[39], J. Fang[1,a], S. S. Fang[1], X. Fang[46,a], Y. Fang[1], R. Farinelli[21A,21B], L. Fava[49B,49C], F. Feldbauer[22], G. Felici[20A], C. Q. Feng[46,a], E. Fioravanti[21A], M. Fritsch[14,22], C. D. Fu[1], Q. Gao[1], X. L. Gao[46,a], Y. Gao[39], Z. Gao[46,a], I. Garzia[21A], K. Goetzen[10], L. Gong[30], W. X. Gong[1,a], W. Gradl[22], M. Greco[49A,49C], M. H. Gu[1,a], Y. T. Gu[12], Y. H. Guan[1], A. Q. Guo[1], L. B. Guo[28], R. P. Guo[1], Y. Guo[1], Y. P. Guo[22], Z. Haddadi[25], A. Hafner[22], S. Han[51], X. Q. Hao[15], F. A. Harris[42], K. L. He[1], F. H. Heinsius[4], T. Held[4], Y. K. Heng[1,a], T. Holtmann[4], Z. L. Hou[1], C. Hu[28], H. M. Hu[1], J. F. Hu[49A,49C], T. Hu[1,a], Y. Hu[1], G. S. Huang[46,a], J. S. Huang[15], X. T. Huang[33], X. Z. Huang[29], Z. L. Huang[27], T. Hussain[48], W. Ikegami Andersson[50], Q. Ji[1], Q. P. Ji[15], X. B. Ji[1], X. L. Ji[1,a], L. W. Jiang[51], X. S. Jiang[1,a], X. Y. Jiang[30], J. B. Jiao[33], Z. Jiao[17], D. P. Jin[1,a], S. Jin[1], T. Johansson[50], A. Julin[43], N. Kalantar-Nayestanaki[25], X. L. Kang[1], X. S. Kang[30], M. Kavatsyuk[25], B. C. Ke[5], P. Kiese[22], R. Kliemt[10], B. Kloss[22], O. B. Kolcu[40B,h], B. Kopf[4], M. Kornicer[42], A. Kupsc[50], W. Kühn[24], J. S. Lange[24], M. Lara[19], P. Larin[14], L. Lavezzi[49C,1], H. Leithoff[22], C. Leng[49C], C. Li[50], Cheng Li[46,a], D. M. Li[53], F. Li[1,a], F. Y. Li[31], G. Li[1], H. B. Li[1], H. J. Li[1], J. C. Li[1], Jin Li[32], K. Li[13], K. Li[33], Lei Li[3], P. R. Li[7,41], Q. Y. Li[33], T. Li[33], W. D. Li[1], W. G. Li[1], X. L. Li[33], X. N. Li[1,a], X. Q. Li[30], Y. B. Li[2], Z. B. Li[38], H. Liang[46,a], Y. F. Liang[36], Y. T. Liang[24], G. R. Liao[11], D. X. Lin[14], B. Liu[34], B. J. Liu[1], C. X. Liu[1], D. Liu[46,a], F. H. Liu[35], Fang Liu[1], Feng Liu[6], H. B. Liu[12], H. H. Liu[1], H. H. Liu[16], H. M. Liu[1], J. Liu[1], J. B. Liu[46,a], J. P. Liu[51], J. Y. Liu[1], K. Liu[39], K. Y. Liu[27], L. D. Liu[31], P. L. Liu[1,a], Q. Liu[41], S. B. Liu[46,a], X. Liu[26], Y. B. Liu[30], Y. Y. Liu[30], Z. A. Liu[1,a], Zhiqing Liu[22], H. Loehner[25], X. C. Lou[1,a,g], H. J. Lu[17], J. G. Lu[1,a], Y. Lu[1], Y. P. Lu[1,a], C. L. Luo[28], M. X. Luo[52], T. Luo[42], X. L. Luo[1,a], X. R. Lyu[41], F. C. Ma[27], H. L. Ma[1], L. L. Ma[33], M. M. Ma[1], Q. M. Ma[1], T. Ma[1], X. N. Ma[30], X. Y. Ma[1,a], Y. M. Ma[33], F. E. Maas[14], M. Maggiora[49A,49C], Q. A. Malik[48], Y. J. Mao[31], Z. P. Mao[1], S. Marcello[49A,49C], J. G. Messchendorp[25], G. Mezzadri[21B], J. Min[1,a], T. J. Min[1], R. E. Mitchell[19], X. H. Mo[1,a], Y. J. Mo[6], C. Morales Morales[14], N. Yu. Muchnoi[9,e], H. Muramatsu[43], P. Musiol[4], Y. Nefedov[23], F. Nerling[10], I. B. Nikolaev[9,e], Z. Ning[1,a], S. Nisar[8], S. L. Niu[1,a], X. Y. Niu[1], S. L. Olsen[32], Q. Ouyang[1,a], S. Pacetti[20B], Y. Pan[46,a], P. Patteri[20A], M. Pelizaeus[4], H. P. Peng[46,a], K. Peters[10,i], J. Pettersson[50], J. L. Ping[28], R. G. Ping[1], R. Poling[43], V. Prasad[1], H. R. Qi[2], M. Qi[29], S. Qian[1,a], C. F. Qiao[41], L. Q. Qin[33], N. Qin[51], X. S. Qin[1], Z. H. Qin[1,a], J. F. Qiu[1], K. H. Rashid[48], C. F. Redmer[22], M. Ripka[22], G. Rong[1], Ch. Rosner[14], X. D. Ruan[12], A. Sarantsev[23,f], M. Savrié[21B], C. Schnier[4], K. Schoenning[50], W. Shan[31], M. Shao[46,a], C. P. Shen[2], P. X. Shen[30], X. Y. Shen[1], H. Y. Sheng[1], W. M. Song[1], X. Y. Song[1], S. Sosio[49A,49C], S. Spataro[49A,49C], G. X. Sun[1], J. F. Sun[15], S. S. Sun[1], X. H. Sun[1], Y. J. Sun[46,a], Y. Z. Sun[1], Z. J. Sun[1,a], Z. T. Sun[19], C. J. Tang[36], X. Tang[1], I. Tapan[40C], E. H. Thorndike[44], M. Tiemens[25], I. Uman[40D], G. S. Varner[42], B. Wang[30], B. L. Wang[41], D. Wang[31], D. Y. Wang[31], K. Wang[1,a], L. L. Wang[1], L. S. Wang[1], M. Wang[33], P. Wang[1], P. L. Wang[1], W. Wang[1,a], W. P. Wang[46,a], X. F. Wang[39], Y. Wang[37], Y. D. Wang[14], Y. F. Wang[1,a], Y. Q. Wang[22], Z. Wang[1,a], Z. G. Wang[1,a], Z. H. Wang[46,a], Z. Y. Wang[1], Z. Y. Wang[1], T. Weber[22], D. H. Wei[11], P. Weidenkaff[22], S. P. Wen[1], U. Wiedner[4], M. Wolke[50], L. H. Wu[1], L. J. Wu[1], Z. Wu[1,a], L. Xia[46,a], L. G. Xia[39], Y. Xia[18], D. Xiao[1], H. Xiao[47], Z. J. Xiao[28], Y. G. Xie[1,a], Yuehong Xie[6], Q. L. Xiu[1,a], G. F. Xu[1], J. J. Xu[1], L. Xu[1], Q. J. Xu[13], Q. N. Xu[41], X. P. Xu[37], L. Yan[49A,49C], W. B. Yan[46,a], W. C. Yan[46,a], Y. H. Yan[18], H. J. Yang[34,j], H. X. Yang[1], L. Yang[51], Y. X. Yang[11], M. Ye[1,a], M. H. Ye[7], J. H. Yin[1], Z. Y. You[38], B. X. Yu[1,a], C. X. Yu[30], J. S. Yu[26], C. Z. Yuan[1], Y. Yuan[1], A. Yuncu[40B,b], A. A. Zafar[48], Y. Zeng[18], Z. Zeng[46,a], B. X. Zhang[1], B. Y. Zhang[1,a], C. C. Zhang[1], D. H. Zhang[1], H. H. Zhang[38], H. Y. Zhang[1,a], J. Zhang[1], J. J. Zhang[1], J. L. Zhang[1], J. Q. Zhang[1], J. W. Zhang[1,a], J. Y. Zhang[1], J. Z. Zhang[1], K. Zhang[1], L. Zhang[1], S. Q. Zhang[30], X. Y. Zhang[33], Y. Zhang[1], Y. Zhang[1], Y. H. Zhang[1,a], Y. N. Zhang[41], Y. T. Zhang[46,a], Yu Zhang[41], Z. H. Zhang[6], Z. P. Zhang[46], Z. Y. Zhang[51], G. Zhao[1], J. W. Zhao[1,a], J. Y. Zhao[1], J. Z. Zhao[1,a], Lei Zhao[46,a], Ling Zhao[1], M. G. Zhao[30], Q. Zhao[1], Q. W. Zhao[1], S. J. Zhao[53], T. C. Zhao[1], Y. B. Zhao[1,a], Z. G. Zhao[46,a], A. Zhemchugov[23,c], B. Zheng[47], J. P. Zheng[1,a], W. J. Zheng[33], Y. H. Zheng[41], B. Zhong[28], L. Zhou[1,a], X. Zhou[51], X. K. Zhou[46,a], X. R. Zhou[46,a], X. Y. Zhou[1], K. Zhu[1], K. J. Zhu[1,a], S. Zhu[1], S. H. Zhu[45], X. L. Zhu[39], Y. C. Zhu[46,a], Y. S. Zhu[1], Z. A. Zhu[1], J. Zhuang[1,a], L. Zotti[49A,49C], B. S. Zou[1], J. H. Zou[1]

(BESIII Collaboration)

[1] *Institute of High Energy Physics, Beijing 100049, People's Republic of China*

[2] *Beihang University, Beijing 100191, People's Republic of China*
[3] *Beijing Institute of Petrochemical Technology, Beijing 102617, People's Republic of China*
[4] *Bochum Ruhr-University, D-44780 Bochum, Germany*
[5] *Carnegie Mellon University, Pittsburgh, Pennsylvania 15213, USA*
[6] *Central China Normal University, Wuhan 430079, People's Republic of China*
[7] *China Center of Advanced Science and Technology, Beijing 100190, People's Republic of China*
[8] *COMSATS Institute of Information Technology, Lahore, Defence Road, Off Raiwind Road, 54000 Lahore, Pakistan*
[9] *G.I. Budker Institute of Nuclear Physics SB RAS (BINP), Novosibirsk 630090, Russia*
[10] *GSI Helmholtzcentre for Heavy Ion Research GmbH, D-64291 Darmstadt, Germany*
[11] *Guangxi Normal University, Guilin 541004, People's Republic of China*
[12] *Guangxi University, Nanning 530004, People's Republic of China*
[13] *Hangzhou Normal University, Hangzhou 310036, People's Republic of China*
[14] *Helmholtz Institute Mainz, Johann-Joachim-Becher-Weg 45, D-55099 Mainz, Germany*
[15] *Henan Normal University, Xinxiang 453007, People's Republic of China*
[16] *Henan University of Science and Technology, Luoyang 471003, People's Republic of China*
[17] *Huangshan College, Huangshan 245000, People's Republic of China*
[18] *Hunan University, Changsha 410082, People's Republic of China*
[19] *Indiana University, Bloomington, Indiana 47405, USA*
[20] *(A)INFN Laboratori Nazionali di Frascati, I-00044, Frascati, Italy; (B)INFN and University of Perugia, I-06100, Perugia, Italy*
[21] *(A)INFN Sezione di Ferrara, I-44122, Ferrara, Italy; (B)University of Ferrara, I-44122, Ferrara, Italy*
[22] *Johannes Gutenberg University of Mainz, Johann-Joachim-Becher-Weg 45, D-55099 Mainz, Germany*
[23] *Joint Institute for Nuclear Research, 141980 Dubna, Moscow region, Russia*
[24] *Justus-Liebig-Universitaet Giessen, II. Physikalisches Institut, Heinrich-Buff-Ring 16, D-35392 Giessen, Germany*
[25] *KVI-CART, University of Groningen, NL-9747 AA Groningen, The Netherlands*
[26] *Lanzhou University, Lanzhou 730000, People's Republic of China*
[27] *Liaoning University, Shenyang 110036, People's Republic of China*
[28] *Nanjing Normal University, Nanjing 210023, People's Republic of China*
[29] *Nanjing University, Nanjing 210093, People's Republic of China*
[30] *Nankai University, Tianjin 300071, People's Republic of China*
[31] *Peking University, Beijing 100871, People's Republic of China*
[32] *Seoul National University, Seoul, 151-747 Korea*
[33] *Shandong University, Jinan 250100, People's Republic of China*
[34] *Shanghai Jiao Tong University, Shanghai 200240, People's Republic of China*
[35] *Shanxi University, Taiyuan 030006, People's Republic of China*
[36] *Sichuan University, Chengdu 610064, People's Republic of China*
[37] *Soochow University, Suzhou 215006, People's Republic of China*
[38] *Sun Yat-Sen University, Guangzhou 510275, People's Republic of China*
[39] *Tsinghua University, Beijing 100084, People's Republic of China*
[40] *(A)Ankara University, 06100 Tandogan, Ankara, Turkey; (B)Istanbul Bilgi University, 34060 Eyup, Istanbul, Turkey; (C)Uludag University, 16059 Bursa, Turkey; (D)Near East University, Nicosia, North Cyprus, Mersin 10, Turkey*
[41] *University of Chinese Academy of Sciences, Beijing 100049, People's Republic of China*
[42] *University of Hawaii, Honolulu, Hawaii 96822, USA*
[43] *University of Minnesota, Minneapolis, Minnesota 55455, USA*
[44] *University of Rochester, Rochester, New York 14627, USA*
[45] *University of Science and Technology Liaoning, Anshan 114051, People's Republic of China*
[46] *University of Science and Technology of China, Hefei 230026, People's Republic of China*
[47] *University of South China, Hengyang 421001, People's Republic of China*
[48] *University of the Punjab, Lahore-54590, Pakistan*
[49] *(A)University of Turin, I-10125, Turin, Italy; (B)University of Eastern Piedmont, I-15121, Alessandria, Italy; (C)INFN, I-10125, Turin, Italy*

[50] Uppsala University, Box 516, SE-75120 Uppsala, Sweden
[51] Wuhan University, Wuhan 430072, People's Republic of China
[52] Zhejiang University, Hangzhou 310027, People's Republic of China
[53] Zhengzhou University, Zhengzhou 450001, People's Republic of China

[a] Also at State Key Laboratory of Particle Detection and Electronics, Beijing 100049, Hefei 230026, People's Republic of China
[b] Also at Bogazici University, 34342 Istanbul, Turkey
[c] Also at the Moscow Institute of Physics and Technology, Moscow 141700, Russia
[d] Also at the Functional Electronics Laboratory, Tomsk State University, Tomsk, 634050, Russia
[e] Also at the Novosibirsk State University, Novosibirsk, 630090, Russia
[f] Also at the NRC "Kurchatov Institute, PNPI, 188300, Gatchina, Russia
[g] Also at University of Texas at Dallas, Richardson, Texas 75083, USA
[h] Also at Istanbul Arel University, 34295 Istanbul, Turkey
[i] Also at Goethe University Frankfurt, 60323 Frankfurt am Main, Germany
[j] Also at Institute of Nuclear and Particle Physics, Shanghai Key Laboratory for Particle Physics and Cosmology, Shanghai 200240, People's Republic of China

The cross sections of $e^+e^- \to \pi^+\pi^- h_c$ at center-of-mass energies from 3.896 to 4.600 GeV are measured using data samples collected with the BESIII detector operating at the Beijing Electron Positron Collider. The cross sections are found to be of the same order of magnitude as those of $e^+e^- \to \pi^+\pi^- J/\psi$ and $e^+e^- \to \pi^+\pi^-\psi(2S)$, but the line shape is inconsistent with the Y states observed in the latter two modes. Two structures are observed in the $e^+e^- \to \pi^+\pi^- h_c$ cross sections around 4.22 and 4.39 GeV/c^2, which we call $Y(4220)$ and $Y(4390)$, respectively. A fit with a coherent sum of two Breit-Wigner functions results in a mass of $(4218.4^{+5.5}_{-4.5} \pm 0.9)$ MeV/c^2 and a width of $(66.0^{+12.3}_{-8.3} \pm 0.4)$ MeV for the $Y(4220)$, and a mass of $(4391.5^{+6.3}_{-6.8} \pm 1.0)$ MeV/c^2 and a width of $(139.5^{+16.2}_{-20.6} \pm 0.6)$ MeV for the $Y(4390)$, where the first uncertainties are statistical and the second ones systematic. The statistical significance of $Y(4220)$ and $Y(4390)$ is 10σ over one structure assumption.

PACS numbers: 14.40.Rt, 14.40.Pq, 13.66.Bc, 13.25.Gv

In the last decade, a series of charmonium-like states have been observed at e^+e^- colliders. These states challenge the understanding of charmonium spectroscopy as well as QCD calculations [1, 2]. According to potential models, there are five vector charmonium states between the 1D state $\psi(3770)$ and 4.7 GeV/c^2, namely the $3S$, $2D$, $4S$, $3D$, and $5S$ states [1]. From experimental studies, besides the three well-established structures observed in the inclusive hadronic cross section [3], i.e., $\psi(4040)$, $\psi(4160)$, and $\psi(4415)$, five Y states, i.e., $Y(4008)$, $Y(4230)$, $Y(4260)$, $Y(4360)$, and $Y(4660)$ have been reported in initial state radiation (ISR) processes $e^+e^- \to \gamma_{\rm ISR}\pi^+\pi^- J/\psi$ or $e^+e^- \to \gamma_{\rm ISR}\pi^+\pi^-\psi(2S)$ at the B factories [4–11] or in the direct production processes at the CLEO and BESIII experiments [12, 13] The overpopulation of structures in this region and the mismatch of the properties between the potential model prediction and experimental measurements make them good candidates for exotic states. Various scenarios have been proposed, which interpret one or some of them as hybrid states, tetraquark states, or molecular states [14].

The study of charmoniumlike states in different production processes supplies useful information on their properties. The process $e^+e^- \to \pi^+\pi^- h_c$ was first studied by CLEO [15] at center-of-mass (c.m.) energies $\sqrt{s}$ from 4.000 to 4.260 GeV. A 10σ signal at 4.170 GeV and a hint of a rising cross section at 4.260 GeV were observed. Using data samples taken at 13 c.m. energies from 3.900 to 4.420 GeV [16], BESIII reported the measurement of the cross section of $e^+e^- \to \pi^+\pi^- h_c$ [17]. Unlike the line shape of the process $e^+e^- \to \pi^+\pi^- J/\psi$, there is a broad structure in the high energy region with a possible local maximum at around 4.23 GeV in $e^+e^- \to \pi^+\pi^- h_c$. Based on the CLEO measurement at $\sqrt{s} = 4.170$ GeV and the BESIII measurement, two assumptions were made to describe the cross section in Ref. [18]. In both assumptions, a narrow structure exists at around 4.23 GeV, while the situation in the high energy region is unclear due to the lack of experimental data.

In this Letter, we present a follow-up study of $e^+e^- \to \pi^+\pi^- h_c$ at c.m. energies from 3.896 to 4.600 GeV using data samples taken at 79 energy points [19] with the BESIII detector [20]. Two resonant structures are observed at $\sqrt{s} = 4.22$ and 4.39 GeV [hereafter referred to as $Y(4220)$ and $Y(4390)$]. The integrated luminosity at each energy point is measured with an uncertainty of 1.0% using large-angle Bhabha events [21, 22]. There are 17 energy points where the integrated luminosities are larger than 40 pb^{-1} (referred to as "XYZ data sample" hereafter), while the integrated luminosities for the other energy points are smaller than 20 pb^{-1} (referred to as "R-scan data sample" hereafter). The c.m. energies for the XYZ data sample are measured with $e^+e^- \to \gamma_{\rm ISR/FSR}\mu^+\mu^-$ events with an uncertainty of ± 0.8 MeV [23], which is dominated by the systematic uncer-

tainty. A similar method is used for the R-scan data sample with multihadron final states [24].

In this study, the h_c is reconstructed via its electric-dipole transition $h_c \to \gamma\eta_c$ with $\eta_c \to X_i$, where X_i is one of 16 exclusive hadronic final states: $p\bar{p}$, $2(\pi^+\pi^-)$, $2(K^+K^-)$, $\pi^+\pi^-K^+K^-$, $\pi^+\pi^-p\bar{p}$, $3(\pi^+\pi^-)$, $2(\pi^+\pi^-)K^+K^-$, $K^0_SK^\pm\pi^\mp$, $K^0_SK^\pm\pi^\mp\pi^+\pi^-$, $K^+K^-\pi^0$, $p\bar{p}\pi^0$, $K^+K^-\eta$, $\pi^+\pi^-\eta$, $2(\pi^+\pi^-)\eta$, $\pi^+\pi^-\pi^0\pi^0$, and $2(\pi^+\pi^-\pi^0)$. Here, the K^0_S is reconstructed using its decay to $\pi^+\pi^-$, and the π^0 and η from the $\gamma\gamma$ final state.

Monte Carlo (MC) simulated events are used to optimize the selection criteria, determine the detection efficiency, and estimate the possible backgrounds. The simulation of the BESIII detector is based on GEANT4 [25] and includes the geometric description of the BESIII detector and the detector response. For the signal process, we use an MC sample for $e^+e^- \to \pi^+\pi^-h_c$ process generated according to phase space. ISR is simulated with KKMC [26] with a maximum energy for the ISR photon corresponding to the $\pi^+\pi^-h_c$ mass threshold.

We select signal candidates with the same method as that described in Ref. [17]. Figure 1 shows the scatter plot of the invariant mass of the η_c candidate versus the one of the h_c candidate and the invariant mass distribution of $\gamma\eta_c$ in the η_c signal region for the data sample at $\sqrt{s} = 4.416$ GeV. A clear $h_c \to \gamma\eta_c$ signal is observed. The η_c signal region is defined by a mass window around the nominal η_c mass [3], which is within ± 50 MeV/c^2 with efficiency about 84% (± 45 MeV/c^2 with efficiency about 80%) from MC simulation for final states with only charged or K^0_S particles (for those including π^0 or η).

We determine the number of $\pi^+\pi^-h_c$ signal events ($n^{\rm obs}_{h_c}$) from the $\gamma\eta_c$ invariant mass distribution. For the XYZ data sample, the $\gamma\eta_c$ mass spectrum is fitted with the MC simulated signal shape convolved with a Gaussian function to reflect the mass resolution difference between the data and MC simulation, together with a linear background. The fit to the data sample at $\sqrt{s} = 4.416$ GeV is shown in Fig. 1. The tail on the high mass side is due to events with ISR (ISR photon undetected); this is simulated with KKMC in MC simulation, and its fraction is fixed in the fit. For the data samples with large statistics ($\sqrt{s} = 4.226$, 4.258, 4.358, and 4.416 GeV), the fit is applied to the 16 η_c decay modes simultaneously with the number of signal events in each decay mode constrained by the corresponding branching fraction [27]. For the data samples at the other energy points, we fit the mass spectrum summed over all η_c decay modes. For the R-scan data sample, the number of signal events is calculated by counting the entries in the h_c signal region [3.515, 3.535] GeV/c^2 ($n^{\rm sig}$) and the entries in the h_c sideband regions [3.475, 3.495] GeV/c^2 and [3.555, 3.575] GeV/c^2 ($n^{\rm side}$) using the formula $n^{\rm obs}_{h_c} = n^{\rm sig} - f n^{\rm side}$. Here, the scale factor $f = 0.5$ is the ratio of the size of the signal region and the background region, and the background is assumed to be distributed linearly in the region of interest.

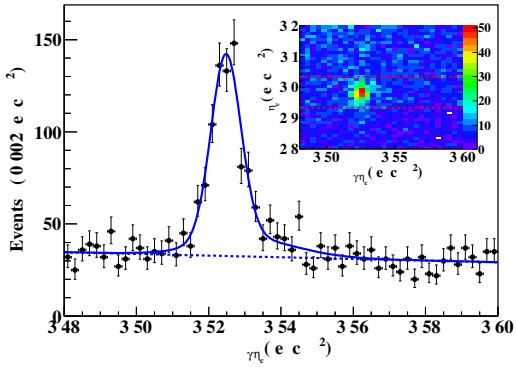

FIG. 1. The $M_{\gamma\eta_c}$ distribution in the η_c signal region of 4.416 GeV data. Points with error bars are the data and the curves are the best fit described in the text. The inset is the scatter plot of the mass of the η_c candidate M_{η_c} versus the mass of the h_c candidate $M_{\gamma\eta_c}$ for the same data sample.

The Born cross section is calculated from

$$\sigma^{\rm B} = \frac{n^{\rm obs}_{h_c}}{\mathcal{L}(1+\delta)|1+\Pi|^2\mathcal{B}_1\sum_{i=1}^{16}\epsilon_i\mathcal{B}_2(i)},$$

where $n^{\rm obs}_{h_c}$ is the number of observed signal events, $\mathcal{L}$ is the integrated luminosity, $(1+\delta)$ is the ISR correction factor, $|1+\Pi|^2$ is the correction factor for vacuum polarization [28], $\mathcal{B}_1$ is the branching fraction of $h_c \to \gamma\eta_c$ [3], ϵ_i and $\mathcal{B}_2(i)$ are the detection efficiency and branching fraction for the i th η_c decay mode [27], respectively. The ISR correction factor is obtained using the QED calculation as described in Ref. [29] and taking the formula used to fit the cross section measured in this analysis after two iterations as input. The Born cross sections are summarized in the Supplemental Material [19] together with all numbers used in the calculation of the Born cross sections. The dressed cross sections (including vacuum polarization effects) are shown in Fig. 2 with dots and squares for the R-scan and XYZ data sample, respectively. The cross sections are of the same order of magnitude as those of the $e^+e^- \to \pi^+\pi^-J/\psi$ and $e^+e^- \to \pi^+\pi^-\psi(2S)$ [4–12], but follow a different line shape. The cross section drops in the high energy region, but more slowly than for the $e^+e^- \to \pi^+\pi^-J/\psi$ process.

Systematic uncertainties in the cross section measurement mainly come from the luminosity measurement, the branching fraction of $h_c \to \gamma\eta_c$, and $\eta_c \to X_i$, the detection efficiency, the ISR correction factor, and the fit. The uncertainty due to the vacuum polarization is negligible. The uncertainty in the integrated luminosity is 1% at each energy point. The uncertainty sources for the detection efficiency include systematic uncertainties in tracking efficiency (1% per track), photon reconstruction (1% per photon), and K^0_S reconstruction (1.2% per K^0_S). Further uncertainties arise from the π^0/η mass win-

dow requirement (1% per π^0/η), the $\chi^2_{\rm 4C}$ requirement, η_c parameters, and line shape, possible intermediate states in the $\pi^\pm h_c$ and $\pi^+\pi^-$ mass spectra, intermediate states in η_c decays (included in the uncertainty from the branching fraction of $\eta_c \to X_i$), and the limited statistics of the MC simulation.

The uncertainty due to the $\chi^2_{\rm 4C}$ requirement is estimated by correcting the helix parameters of the simulated charged tracks to match the resolution found in data, and repeating the analysis [30]. Uncertainties due to the η_c parameters and line shape are estimated by varying them in the MC simulation. When producing MC events for the $e^+e^- \to \pi^+\pi^- h_c$ process through the intermediate states $Z_c(3900)$ or $Z_c(4020)$, the parameters of the $Z_c(3900)$ and $Z_c(4020)$ are fixed to the average values from the published measurements [11, 17, 31–33]. The quantum numbers of both $Z_c(3900)$ and $Z_c(4020)$ are assumed to be $J^P = 1^+$. The differences in the efficiency obtained from phase space MC samples and those with intermediate Z_c states are taken as the uncertainties from possible intermediate states in the $\pi^\pm h_c$ system. The uncertainty from intermediate states in the $\pi^+\pi^-$ system is estimated by reweighting the $\pi^+\pi^-$ mass distribution in the phase space MC sample according to the data, and the resulting difference in the efficiency is considered as uncertainty. The uncertainties due to data and MC differences in the detection efficiency are determined to be between 5.5% and 10.8%, depending on the η_c decay modes and the c.m. energy. Combining the uncertainties for the branching fractions of η_c decays [27], the uncertainties for the average efficiency $\sum_{i=1}^{16} \epsilon_i \mathcal{B}_2(i)$ are between 6.4% and 9.1% depending on the c.m. energy.

The uncertainty in the ISR correction is estimated as described in Ref. [31]. Uncertainties due to the choice of the signal shape, the background shape, the mass resolution, and fit range are estimated by changing the h_c and η_c resonant parameters and line shapes in the MC simulation, changing the background function from a linear to a second-order polynomial, changing the mass resolution difference between the data and the MC simulation by 1 standard deviation, and by extending or shrinking the fit range.

Assuming all of the sources are independent, the total systematic uncertainty in the $\pi^+\pi^- h_c$ cross section measurement is determined to be 9.4%-13.6% depending on the c.m. energy. The uncertainty in $\mathcal{B}_1$ is 11.8% [3], common to all energy points, and quoted separately in the cross section measurement. Altogether, the quadratic sum of the common systematic errors at each energy point accounts for about 95% of the total systematic error.

A maximum likelihood method is used to fit the dressed cross sections to determine the parameters of the resonant structures. The likelihood is constructed taking the fluctuations of the number of signal and background events into account (the definition is described in the Supplemental Material [19]). Assuming that the $\pi^+\pi^- h_c$ signal comes from two resonances, the cross section is parametrized as the coherent sum of two constant width relativistic Breit-Wigner functions, i.e.,

$$\sigma(m) = |B_1(m) \cdot \sqrt{\frac{P(m)}{P(M_1)}} + e^{i\phi} B_2(m) \cdot \sqrt{\frac{P(m)}{P(M_2)}}|^2,$$

where $B_j(m) = \sqrt{12\pi(\Gamma_{ee}\mathcal{B})_j \Gamma_j}/(m^2 - M_j^2 + iM_j\Gamma_j)$ with $j = 1$ or 2 is the Breit-Wigner function, and $P(m)$ is the three-body phase space factor. The masses M_j, the total widths Γ_j, the products of the electronic partial width and the branching fraction to $\pi^+\pi^- h_c$ $(\Gamma_{ee}\mathcal{B})_j$, and the relative phase ϕ between the two Breit-Wigner functions are free parameters in the fit. Only the statistical uncertainty is considered in the fit. There are two solutions from the fit, one of them is shown in Fig. 2. The second solution is very close to the one shown here. This can been proved analytically using Eq.(9) in Ref. [34], which relates the two solutions from the fit when a sum of two coherent Breit-Wigner functions is used. The parameters determined from the fit are $M_1 = (4218.4^{+5.5}_{-4.5})$ MeV/c^2, $\Gamma_1 = (66.0^{+12.3}_{-8.3})$ MeV, and $(\Gamma_{ee}\mathcal{B})_1 = (4.6^{+2.9}_{-1.4})$ eV for $Y(4220)$, $M_2 = (4391.5^{+6.3}_{-6.8})$ MeV/c^2, $\Gamma_2 = (139.5^{+16.2}_{-20.6})$ MeV, and $(\Gamma_{ee}\mathcal{B})_2 = (11.6^{+5.0}_{-4.4})$ eV for $Y(4390)$. The relative phase ϕ is $(3.1^{+0.7}_{-0.9})$ rad. The correlation matrix of the fit parameters shows large correlation between the $(\Gamma_{ee}\mathcal{B})_j$ and ϕ (see Supplemental Material [19]).

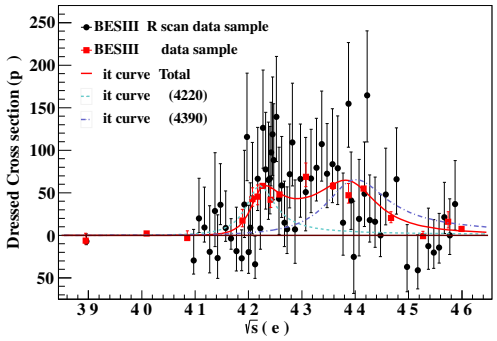

FIG. 2. Fit to the dressed cross section of $e^+e^- \to \pi^+\pi^- h_c$ with the coherent sum of two Breit-Wigner functions (solid curve). The dash (dash-dot) curve shows the contribution from the two structures $Y(4220)$ [$Y(4390)$]. The dots with error bars are the cross sections for the R-scan data sample, the squares with error bars are the cross sections for the XYZ data sample. Here the error bars are statistical uncertainty only.

The likelihood contours in the mass and width planes for $Y(4220)$ and $Y(4390)$ are shown in Fig. 3, together with the positions of $Y(4230)$, $Y(4260)$, $Y(4360)$, and $\psi(4415)$ with the parameters taken from the latest PDG average [3]. The low-lying resonance from the study of $e^+e^- \to \pi^+\pi^- J/\psi$ at BESIII [35], marked as $Y(4260)^{\rm BESIII}$ in the plot, is also compared. $Y(4260)$, $Y(4360)$, and $\psi(4415)$ are located out-

side the 3σ contours, while $Y(4230)$ and $Y(4260)^{\rm BESIII}$ are overlapped with the 3σ contour of $Y(4220)$.

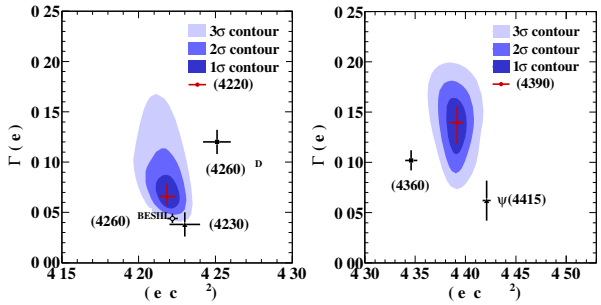

FIG. 3. The likelihood contours in the mass and width planes for $Y(4220)$ (*left panel*) and $Y(4390)$ (*right panel*). The filled areas are up to 3σ likelihood contours and the dots with error bars are the locations of Y or ψ states. The parameters of $Y(4260)^{\rm PDG}$ are taken from the PDG average [3] and $Y(4260)^{\rm BESIII}$ from the measurement of $e^+e^- \to \pi^+\pi^- J/\psi$ at BESIII [35].

Fitting the dressed cross section with only one resonance yields a worse result, the change of the likelihood value from two resonances to one resonance is $[\Delta(-2\ln L) = 113.5]$. Taking the change in the number of degrees of freedom (4) into account, the significance for the assumption of two resonant structures over the assumption of one resonant structure is 10σ. The fit with the coherent sum of one Breit-Wigner function and a phase space term gives a worse result as well, the change of the likelihood value is $[\Delta(-2\ln L) = 66.8]$. We also fit the cross section with the coherent sum of three Breit-Wigner functions, or the coherent sum of two Breit-Wigner functions and a phase space term. Both assumptions improve the fit quality, but the significances of the third resonance and the phase space term are only 2.6σ and 2.9σ, respectively.

The systematic uncertainties in the resonance parameters mainly come from the absolute c.m. energy measurement, the c.m. energy spread, and the systematic uncertainty on the cross section measurement. The uncertainty from the c.m. energy measurement includes the uncertainty of the c.m. energy and the assumption made in the measurement for the R-scan data sample. Because of the low statistics at each energy point in the R-scan data sample, we approximate the difference between the requested and the actual c.m. energy by a common constant. To assess the systematic uncertainty connected with this assumption, we replace the constant by a c.m. energy-dependent second-order polynomial. The systematic uncertainty of the c.m. energy is common for all the energy points in the two data samples and will propagate to the mass measurement (0.8 MeV). The changes on the parameters are taken as uncertainty. The uncertainty from c.m. energy spread is estimated by convoluting the fit formula with a Gaussian function with a width of 1.6 MeV, which is beam spread, measured by the Beam Energy Measurement System [36]. The uncertainty from the cross section measurement is divided into two parts. The first one is uncorrelated among the different c.m. energy points and comes mainly from the fit to the $\gamma\eta_c$ invariant mass spectrum to determine the signal yields. The corresponding uncertainty is estimated by including the uncertainty in the fit to the cross section, and taking the differences on the parameters as uncertainties. The second part includes all the other sources, is common for all data points (14.8%), and only affects the $\Gamma_{ee}\mathcal{B}$ measurement. Table I summarizes the systematic uncertainty in the resonance parameters.

In summary, we measure the $e^+e^- \to \pi^+\pi^- h_c$ Born cross section using data at 79 c.m. energy points from 3.896 to 4.600 GeV. Assuming the $\pi^+\pi^- h_c$ events come from two resonances, we obtain $M = (4218.4^{+5.5}_{-4.5} \pm 0.9)$ MeV/c^2, $\Gamma = (66.0^{+12.3}_{-8.3} \pm 0.4)$ MeV, and $(\Gamma_{ee}\mathcal{B}) = (4.6^{+2.9}_{-1.4} \pm 0.8)$ eV for $Y(4220)$, and $M = (4391.5^{+6.3}_{-6.8} \pm 1.0)$ MeV/c^2, $\Gamma = (139.5^{+16.2}_{-20.6} \pm 0.6)$ MeV, and $(\Gamma_{ee}\mathcal{B}) = (11.6^{+5.0}_{-4.4} \pm 1.9)$ eV for $Y(4390)$, with a relative phase of $\phi = (3.1^{+0.7}_{-0.9} \pm 0.2)$ rad. The first errors are statistical and the second are systematic. The parameters of these structures are different from those of $Y(4260)$, $Y(4360)$, and $\psi(4415)$ [3]. The resonance parameters of $Y(4220)$ are consistent with those of the resonance observed in $e^+e^- \to \omega\chi_{c0}$ [13].

The two resonances observed in $e^+e^- \to \pi^+\pi^- h_c$ process are located in the mass region between 4.2 and 4.4 GeV/c^2, where the vector charmonium hybrid states are predicted from various QCD calculations [37–39]. The mass of $Y(4220)$ is lower than that of $Y(4260)$ observed in the $e^+e^- \to \pi^+\pi^- J/\psi$ process. The smaller mass is consistent with some of the theoretical calculations for the mass of $Y(4260)$ when explaining it as a $D_1\bar{D}$ molecule [40, 41].

The BESIII Collaboration thanks the staff of BEPCII and the IHEP computing center for their strong support. This work is supported in part by National Key Basic Research Program of China under Contract No. 2015CB856700; National Natural Science Foundation of China (NSFC) under Contracts Nos. 11235011, 11322544, 11335008, 11425524; the Chinese Academy of Sciences (CAS) Large-Scale Scientific Facility Program; the CAS Center for Excellence in Particle Physics (CCEPP); the Collaborative Innovation Center for Particles and Interactions (CICPI); Joint Large-Scale Scientific Facility Funds of the NSFC and CAS under Contracts Nos. U1232201, U1332201; CAS under Contracts Nos. KJCX2-YW-N29, KJCX2-YW-N45; 100 Talents Program of CAS; National 1000 Talents Program of China; INPAC and Shanghai Key Laboratory for Particle Physics and Cosmology; German Research Foundation DFG under Contracts Nos. Collaborative Research Center CRC 1044, FOR 2359; Istituto Nazionale di Fisica Nucleare, Italy; Joint Large-Scale Scientific Facility Funds of the NSFC and CAS under Contract No. U1532257; Joint Large-Scale Scientific Facility Funds of the NSFC and CAS under Contract No. U1532258; Koninklijke Nederlandse Akademie van Wetenschappen (KNAW) under Contract No. 530-4CDP03; Ministry of Development of Turkey under Contract No.

TABLE I. The systematic uncertainty in the measurement of the resonance parameters. c.m. energy$_{1,2}$ represent the uncertainty from the systematic uncertainty of c.m. energy measurement and the assumption made in the c.m. energy measurement for R-scan data sample, respectively. Cross section$_{a(b)}$ represents the uncertainty from the systematic uncertainties of the cross section measurement which are uncorrelated (common) in each energy point.

Sources	$Y(4220)$			$Y(4390)$			ϕ (rad)
	M (MeV/c^2)	Γ (MeV)	($\Gamma_{ee}\mathcal{B}$) (eV)	M (MeV/c^2)	Γ (MeV)	($\Gamma_{ee}\mathcal{B}$) (eV)	
c.m. energy$_{1(2)}$	0.8(0.1)	$-$(0.1)	$-$(0.2)	0.8(0.1)	$-$(0.2)	$-$(0.3)	$-$(0.1)
c.m. energy spread	0.1	0.3	0.3	0.1	0.1	0.7	0.1
Cross section$_{a(b)}$	0.1($-$)	$-$($-$)	0.2(0.7)	0.6($-$)	0.5($-$)	0.4(1.7)	0.1($-$)
Total	0.9	0.4	0.8	1.0	0.6	1.9	0.2

DPT2006K-120470; NSFC under Contract No. 11275266; The Swedish Resarch Council; U. S. Department of Energy under Contracts Nos. DE-FG02-05ER41374, DE-SC-0010504, de-sc0012069, DESC0010118; U.S. National Science Foundation; University of Groningen (RuG) and the Helmholtzzentrum fuer Schwerionenforschung GmbH (GSI), Darmstadt; WCU Program of National Research Foundation of Korea under Contract No. R32-2008-000-10155-0.

[1] For a recent review, see N. Brambilla *et al.*, Eur. Phys. J. C **71**, 1534 (2011).
[2] R. A. Briceno *et al.*, Chin. Phys. C **40(4)**, 042001 (2016).
[3] K. A. Olive *et al.* (Particle Data Group), Chin. Phys. C **38(9)**, 090001 (2014); C. Patrignani *et al.* (Particle Data Group), Chin. Phys. C **40(10)**, 100001 (2016).
[4] B. Aubert *et al.* (BaBar Collaboration), Phys. Rev. Lett. **95**, 142001 (2005).
[5] C. Z. Yuan *et al.* (Belle Collaboration), Phys. Rev. Lett. **99**, 182004 (2007).
[6] B. Aubert *et al.* (BaBar Collaboration), Phys. Rev. Lett. **98**, 212001 (2007).
[7] X. L. Wang *et al.* (Belle Collaboration), Phys. Rev. Lett. **99**, 142002 (2007).
[8] J. P. Lees *et al.* (BaBar Collaboration), Phys. Rev. D **89**, 111103 (2014).
[9] X. L. Wang *et al.* (Belle Collaboration), Phys. Rev. D **91**, 112007 (2015).
[10] J. P. Lees *et al.* (BaBar Collaboration), Phys. Rev. D **86**, 051102(R) (2012).
[11] Z. Q. Liu *et al.* (Belle Collaboration), Phys. Rev. Lett. **110**, 252002 (2013).
[12] T. E. Coan *et al.* (CLEO Collaboration), Phys. Rev. Lett. **96**, 162003 (2006).
[13] M. Ablikim *et al.* (BESIII Collaboration), Phys. Rev. Lett. **114**, 092003 (2015).
[14] H. X. Chen, W. Chen, X. Liu, and S. L. Zhu, Phys. Rep. **639**, 1 (2016).
[15] T. K. Pedlar *et al.* (CLEO Collaboration), Phys. Rev. Lett. **107**, 041803 (2011).
[16] The data samples are the same as those used in this study except at 4.420 GeV. At 4.420 GeV, more data has been collected and analysed. Besides, the CM energies at all energy points have been remeasured using $e^+e^- \to \gamma_{\rm ISR/FSR}\mu^+\mu^-$ events, and found to be a few MeV smaller.
[17] M. Ablikim *et al.* (BESIII Collaboration), Phys. Rev. Lett. **111**, 242001 (2013).
[18] C. Z. Yuan, Chin. Phys. C **38(4)**, 043001 (2014).
[19] See supplemental material at [URL will be inserted by publisher] for a summary of number of signal events, luminosity, and Born cross section at each energy point, the definition of the likelihood used in the fit to the dressed cross section, and the correlation matrix of the fit parameters from the fit.
[20] M. Ablikim *et al.* (BESIII Collaboration), Nucl. Instrum. Meth. A **614**, 345 (2010).
[21] M. Ablikim *et al.* (BESIII Collaboration), Chin. Phys. C **39(9)**, 093001 (2015).
[22] M. Ablikim *et al.* (BESIII Collaboration), arXiv:1702.04977.
[23] M. Ablikim *et al.* (BESIII Collaboration), Chin. Phys. C **40(6)**, 063001 (2016).
[24] M. Ablikim *et al.* (BESIII Collaboration), "Measurement of the center-of-mass energies for R scan experiment", paper in preparation.
[25] S. Agostinelli *et al.* (GEANT4 Collaboration), Nucl. Instrum. Meth. A **506**, 250 (2003).
[26] S. Jadach, B. F. L. Ward and Z. Was, Comp. Phys. Commu. **130**, 260 (2000); Phys. Rev. D **63**, 113009 (2001).
[27] M. Ablikim *et al.*, (BESIII Collaboration), Phys. Rev. D **86**, 092009 (2012).
[28] S. Actis *et al.*, Eur. Phys. J. C 66, 585 (2010).
[29] E. A. Kuraev and V. S. Fadin, Sov. J. Nucl. Phys. **41**, 466 (1985) [Yad. Fiz. **41**, 733 (1985).]
[30] M. Ablikim *et al.* (BESIII Collaboration), Phys. Rev. D **87**, 012002 (2013).
[31] M. Ablikim *et al.* (BESIII Collaboration), Phys. Rev. Lett. **110**, 252001 (2013).
[32] T. Xiao, S. Dobbs, A. Tomaradze and K. K. Seth, Phys. Lett. B **727**, 366 (2013).
[33] M. Ablikim *et al.* (BESIII Collaboration), Phys. Rev. Lett. **112**, 022001 (2014).
[34] K. Zhu, X. H. Mo, C. Z. Yuan and P. Wang, Int. J. Mod. Phys. A **26**, 4511 (2011).
[35] M. Ablikim *et al.* BESIII Collaboration, arXiv:1611.01317[hep-ex].
[36] E. V. Abakumova *et al.*, Nucl. Instrum. Meth. A **659**, 21 (2011).
[37] L. Liu *et al.* (Hadron Spectrum Collaboration), J. High Energy Phys. **07**, 126 (2012).
[38] T. Barnes, F. E. Close, and E. S. Swanson, Phys. Rev. D **52**, 5242 (1995); P. Guo, A. P. Szczepaniak, G. Galata, A. Vassallo and E. Santopinto, Phys. Rev. D **78**, 056003 (2008); Yu. S. Kalashnikova and A. V. Nefediev, Phys. Rev. D **77**, 054025 (2008).
[39] Y. Chen, W. F. Chiu, M. Gong, L. C. Gui, and Z. F. Liu, Chin.

Phys. C **40(8)**, 081002 (2016).
[40] M. Cleven, Q. Wang, F. K. Guo, C. Hanhart, U. G. Meißner, and Q. Zhao, Phys. Rev. D **90**, 074039 (2014).
[41] T. W. Chiu and T. H. Hsieh (TWQCD Collaboration), Phys. Rev. D **73**, 094510 (2006).

Appendices

Cross section of $e^+e^- \to \pi^+\pi^- h_c$

The number of signal events $n_{h_c}^{\rm obs}$, the luminosity $\mathcal{L}$, the product of the initial state radiation correction factor and average efficiency $(1+\delta)\sum_{i=1}^{16}\epsilon_i\mathcal{B}(\eta_c\to X_i)$, the vacuum polarization correction factor $|1+\Pi|^2$, and the Born cross section $\sigma^{\rm B}$ for XYZ data sample and R-scan data sample are summarized in Table II and Table III. The average efficiency is smaller for the R-scan data sample than for the XYZ data sample due to the different methods used in determining the number of signal events.

TABLE II. $e^+e^- \to \pi^+\pi^- h_c$ cross sections from XYZ data sample. The first errors are statistical, and the second ones systematic uncertainty except the uncertainty in $\mathcal{B}(h_c\to\gamma\eta_c)$, and the third errors are from the uncertainty in $\mathcal{B}(h_c\to\gamma\eta_c)$.

$\sqrt{s}$ (GeV)	$\mathcal{L}$ (pb^{-1})	$n_{h_c}^{\rm obs}$	$(1+\delta)\sum_{i=1}^{16}\epsilon_i\mathcal{B}(\eta_c\to X_i)(\%)$	$\lvert1+\Pi\rvert^2$	$\sigma^{\rm B}$ (pb)
3.8962	52.6	$-1.5^{+1.9}_{-0.8}$	0.78	1.049	$-6.8\,^{+8.4}_{-3.7}\pm0.6\pm0.8$
4.0076	482.0	$7.6^{+7.2}_{-4.7}$	1.42	1.044	$2.0\,^{+2.0}_{-1.3}\pm0.3\pm0.2$
4.0855	52.6	$-1.6^{+4.2}_{-1.5}$	1.85	1.052	$-3.1\,^{+8.0}_{-2.9}\pm0.4\pm0.4$
4.1886	43.1	$7.4^{+5.7}_{-3.1}$	1.96	1.056	$16.6^{+12.5}_{-6.8}\pm1.8\pm2.0$
4.2077	54.6	$23.6^{+7.2}_{-4.7}$	1.99	1.057	$40.7^{+12.3}_{-8.0}\pm3.9\pm4.8$
4.2171	54.1	$25.3^{+7.8}_{-5.3}$	2.03	1.057	$43.2^{+13.2}_{-8.9}\pm4.2\pm5.1$
4.2263	1091.7	669 ± 32	2.07	1.056	$55.2\pm2.6\pm6.1\pm6.5$
4.2417	55.6	$25.5^{+8.1}_{-5.6}$	2.17	1.056	$39.9^{+12.5}_{-8.6}\pm3.8\pm4.7$
4.2580	825.7	443 ± 27	2.23	1.054	$46.3\pm2.8\pm5.1\pm5.5$
4.3079	44.9	$34.3^{+8.3}_{-5.8}$	2.22	1.052	$65.0^{+15.6}_{-10.9}\pm6.1\pm7.7$
4.3583	539.8	357 ± 24	2.26	1.051	$55.8\pm3.7\pm6.2\pm6.6$
4.3874	55.2	$30.2^{+8.8}_{-6.1}$	2.30	1.051	$45.5^{+12.9}_{-9.0}\pm4.4\pm5.4$
4.4156	1073.6	685 ± 35	2.28	1.053	$52.1\pm2.7\pm5.9\pm6.1$
4.4671	109.9	$27.1^{+9.7}_{-7.2}$	2.38	1.055	$19.3\,^{+6.9}_{-5.1}\pm2.4\pm2.3$
4.5271	110.0	$-1.3^{+7.5}_{-4.9}$	2.39	1.055	$-0.9\,^{+5.3}_{-3.5}\pm0.1\pm0.1$
4.5745	47.7	$9.2^{+6.8}_{-4.3}$	2.37	1.055	$15.1^{+11.2}_{-7.1}\pm2.1\pm1.8$
4.5995	566.9	$52.0^{+16.9}_{-14.3}$	2.38	1.055	$7.2\,^{+2.3}_{-2.0}\pm0.7\pm0.8$

TABLE III: $e^+e^- \to \pi^+\pi^- h_c$ cross sections in R-scan data sample. The errors are statistical only. The systematic uncertainty is 18.0%, and common for all energy points.

$\sqrt{s}$ (GeV)	$\mathcal{L}$ (pb^{-1})	$n^{\rm sig}$	$n^{\rm side}$	$n_{h_c}^{\rm obs}$	$(1+\delta)\sum_{i=1}^{16}\epsilon_i\mathcal{B}(\eta_c\to X_i)(\%)$	$\lvert1+\Pi\rvert^2$	$\sigma^{\rm B}$ (pb)
4.0974	7.254	0	3	$-1.5^{+1.9}_{-0.8}$	1.37	1.052	$-28.0^{+34.6}_{-15.3}$
4.1074	7.146	1	0	$1.0^{+2.4}_{-0.8}$	1.38	1.052	$18.9^{+44.7}_{-15.6}$
4.1174	7.648	1	1	$0.5^{+2.6}_{-0.9}$	1.39	1.052	$8.8^{+45.1}_{-16.3}$
4.1274	7.207	1	4	$-1.0^{+2.8}_{-1.3}$	1.40	1.053	$-18.5^{+51.5}_{-23.4}$
4.1374	7.268	4	5	$1.5^{+3.6}_{-2.2}$	1.41	1.052	$27.2^{+65.0}_{-39.9}$
4.1424	7.774	1	5	$-1.5^{+2.9}_{-1.4}$	1.42	1.052	$-25.3^{+48.1}_{-22.9}$
4.1474	7.662	2	0	$2.0^{+2.7}_{-1.3}$	1.43	1.053	$34.0^{+45.8}_{-21.9}$
4.1574	7.954	1	1	$0.5^{+2.6}_{-0.9}$	1.45	1.054	$8.1^{+41.5}_{-14.9}$
4.1674	18.008	2	5	$-0.5^{+3.1}_{-1.7}$	1.46	1.054	$-3.5^{+22.2}_{-11.9}$
4.1774	7.309	1	4	$-1.0^{+2.8}_{-1.3}$	1.45	1.055	$-17.5^{+48.8}_{-22.2}$
4.1874	7.560	0	3	$-1.5^{+1.9}_{-0.8}$	1.45	1.056	$-25.5^{+31.5}_{-13.9}$
4.1924	7.503	4	4	$2.0^{+3.5}_{-2.1}$	1.45	1.057	$34.2^{+60.3}_{-36.6}$
4.1974	7.582	8	3	$6.5^{+4.2}_{-2.9}$	1.45	1.057	$109.4^{+70.7}_{-48.6}$
4.2004	6.815	1	4	$-1.0^{+2.8}_{-1.3}$	1.46	1.057	$-18.7^{+52.0}_{-23.6}$
4.2034	7.638	2	3	$0.5^{+3.0}_{-1.5}$	1.46	1.057	$8.3^{+49.9}_{-25.4}$

Continued on next page

TABLE III – continued from previous page

$\sqrt{s}$ (GeV)	$\mathcal{L}$ (pb^{-1})	$n^{\rm sig}$	$n^{\rm side}$	$n_{h_c}^{\rm obs}$	$(1+\delta)\sum_{i=1}^{16}\epsilon_i\mathcal{B}(\eta_c\to X_i)$ (%)	$\lvert 1+\Pi\rvert^2$	$\sigma^{\rm B}$ (pb)
4.2074	7.678	5	5	$2.5^{+3.8}_{-2.4}$	1.47	1.057	$41.1^{+62.1}_{-39.7}$
4.2124	7.768	0	4	$-2.0^{+2.0}_{-1.0}$	1.48	1.056	$-32.4^{+31.6}_{-15.5}$
4.2174	7.935	5	2	$4.0^{+3.6}_{-2.3}$	1.49	1.057	$62.9^{+57.0}_{-35.4}$
4.2224	8.212	2	3	$0.5^{+3.0}_{-1.5}$	1.50	1.057	$7.5^{+45.3}_{-23.0}$
4.2274	8.193	9	2	$8.0^{+4.3}_{-3.0}$	1.52	1.056	$119.6^{+64.4}_{-45.0}$
4.2324	8.273	8	6	$5.0^{+4.3}_{-3.0}$	1.53	1.056	$73.4^{+63.5}_{-44.2}$
4.2374	7.830	7	6	$4.0^{+4.2}_{-2.8}$	1.54	1.056	$61.7^{+64.2}_{-43.8}$
4.2404	8.571	7	5	$4.5^{+4.1}_{-2.8}$	1.54	1.056	$63.2^{+57.9}_{-39.3}$
4.2424	8.487	7	1	$6.5^{+3.9}_{-2.6}$	1.54	1.056	$92.1^{+55.7}_{-37.0}$
4.2454	8.554	10	4	$8.0^{+4.6}_{-3.3}$	1.55	1.055	$112.5^{+63.8}_{-45.7}$
4.2474	8.596	9	6	$6.0^{+4.5}_{-3.2}$	1.55	1.055	$83.9^{+62.6}_{-44.4}$
4.2524	8.657	12	5	$9.5^{+4.9}_{-3.6}$	1.55	1.054	$132.0^{+67.4}_{-49.8}$
4.2574	8.880	7	8	$3.0^{+4.3}_{-2.9}$	1.55	1.054	$40.6^{+57.5}_{-39.7}$
4.2624	8.629	6	4	$4.0^{+3.9}_{-2.6}$	1.55	1.053	$55.7^{+54.5}_{-35.7}$
4.2674	8.548	3	4	$1.0^{+3.3}_{-1.9}$	1.55	1.053	$14.0^{+46.5}_{-26.5}$
4.2724	8.567	3	5	$0.5^{+3.4}_{-2.0}$	1.56	1.053	$7.0^{+47.0}_{-27.3}$
4.2774	8.723	7	4	$5.0^{+4.1}_{-2.8}$	1.56	1.053	$68.3^{+55.7}_{-37.6}$
4.2824	8.596	11	7	$7.5^{+4.8}_{-3.5}$	1.57	1.053	$103.6^{+66.2}_{-48.5}$
4.2874	9.010	6	11	$0.5^{+4.2}_{-2.9}$	1.57	1.053	$6.6^{+55.3}_{-38.0}$
4.2974	8.453	8	7	$4.5^{+4.4}_{-3.1}$	1.57	1.052	$63.0^{+61.1}_{-42.8}$
4.3074	8.599	8	9	$3.5^{+4.4}_{-3.1}$	1.57	1.052	$48.2^{+61.2}_{-43.2}$
4.3174	9.342	8	6	$5.0^{+4.3}_{-3.0}$	1.57	1.052	$63.5^{+54.9}_{-38.3}$
4.3274	8.657	7	3	$5.5^{+4.0}_{-2.7}$	1.57	1.051	$75.5^{+55.4}_{-37.1}$
4.3374	8.700	9	3	$7.5^{+4.4}_{-3.1}$	1.58	1.051	$102.0^{+59.2}_{-41.6}$
4.3474	8.542	7	4	$5.0^{+4.1}_{-2.8}$	1.59	1.051	$68.8^{+56.1}_{-37.9}$
4.3574	8.063	8	5	$5.5^{+4.3}_{-3.0}$	1.60	1.051	$79.5^{+61.9}_{-42.9}$
4.3674	8.498	8	5	$5.5^{+4.3}_{-3.0}$	1.61	1.052	$74.9^{+58.3}_{-40.5}$
4.3774	8.158	5	8	$1.0^{+3.9}_{-2.6}$	1.62	1.052	$14.1^{+55.3}_{-36.3}$
4.3874	7.460	10	1	$9.5^{+4.4}_{-3.1}$	1.61	1.051	$147.2^{+68.3}_{-48.6}$
4.3924	7.430	4	3	$2.5^{+3.5}_{-2.1}$	1.61	1.051	$39.0^{+54.2}_{-32.4}$
4.3974	7.178	4	11	$-1.5^{+3.9}_{-2.5}$	1.61	1.052	$-24.2^{+62.2}_{-40.6}$
4.4074	6.352	4	6	$1.0^{+3.6}_{-2.3}$	1.60	1.053	$18.3^{+66.4}_{-41.3}$
4.4174	7.519	5	4	$3.0^{+3.7}_{-2.4}$	1.60	1.053	$46.4^{+57.7}_{-36.6}$
4.4224	7.436	11	2	$10.0^{+4.6}_{-3.3}$	1.60	1.053	$156.2^{+71.9}_{-52.0}$
4.4274	6.788	2	2	$1.0^{+2.9}_{-1.4}$	1.61	1.053	$17.1^{+50.2}_{-24.6}$
4.4374	7.634	3	4	$1.0^{+3.3}_{-1.9}$	1.62	1.055	$15.0^{+49.8}_{-28.4}$
4.4474	7.677	2	4	$0.0^{+3.1}_{-1.6}$	1.63	1.055	$0.0^{+45.6}_{-23.9}$
4.4574	8.724	6	5	$3.5^{+4.0}_{-2.6}$	1.64	1.055	$45.5^{+51.5}_{-34.0}$
4.4774	8.167	7	5	$4.5^{+4.1}_{-2.8}$	1.64	1.055	$62.4^{+57.2}_{-38.8}$
4.4974	7.997	2	9	$-2.5^{+3.3}_{-2.0}$	1.65	1.055	$-35.3^{+47.1}_{-27.7}$
4.5174	8.674	1	8	$-3.0^{+3.0}_{-1.6}$	1.65	1.055	$-38.9^{+39.2}_{-20.9}$
4.5374	9.335	3	8	$-1.0^{+3.5}_{-2.1}$	1.65	1.055	$-12.0^{+42.3}_{-25.8}$
4.5474	8.765	1	5	$-1.5^{+2.9}_{-1.4}$	1.65	1.054	$-19.3^{+36.6}_{-17.5}$
4.5574	8.259	1	4	$-1.0^{+2.8}_{-1.3}$	1.65	1.055	$-13.7^{+38.1}_{-17.3}$
4.5674	8.390	2	1	$1.5^{+2.9}_{-1.4}$	1.64	1.055	$20.2^{+38.7}_{-18.3}$
4.5774	8.545	2	4	$0.0^{+3.1}_{-1.6}$	1.64	1.055	$0.0^{+40.7}_{-21.3}$
4.5874	8.162	4	3	$2.5^{+3.5}_{-2.1}$	1.63	1.055	$34.7^{+48.3}_{-28.9}$

Definition of likelihood function

In the maximum likelihood fit to the dressed cross sections of $e^+e^- \to \pi^+\pi^- h_c$, the likelihood is defined as:

$$L(\mu^{\rm sig}; p) = \prod_{i=1}^{17} L_i(\mu^{\rm sig}; p_i) \prod_{j=1}^{62} L_j(\mu^{\rm sig}; p_j), \tag{1}$$

where $\mu^{\rm sig}$ is the expected number of signal events, p_i and p_j are the parameters in the likelihood functions. L_i and L_j are the likelihood functions for the XYZ and R-scan data samples, respectively.

The likelihood functions for the XYZ and R-scan data samples are defined differently due to the different statistics of the samples. For the XYZ data sample, where the statistics is large, the likelihood function is described by an asymmetric Gaussian function $L_i = G(\mu_i^{\rm sig}; m_i, \sigma_i^{\rm left}, \sigma_i^{\rm right})$,

$$\begin{aligned} G(\mu_i^{\rm sig}; m_i, \sigma_i^{\rm left}, \sigma_i^{\rm right}) \;=\; & \frac{1}{\sqrt{2\pi}(\sigma_i^{\rm left} + \sigma_i^{\rm right})} e^{-\frac{(\mu_i^{\rm sig} - m_i)^2}{2(\sigma_i^{\rm left})^2}}, \mu_i^{\rm sig} < m_i; \\ & \frac{1}{\sqrt{2\pi}(\sigma_i^{\rm left} + \sigma_i^{\rm right})} e^{-\frac{(\mu_i^{\rm sig} - m_i)^2}{2(\sigma_i^{\rm right})^2}}, \mu_i^{\rm sig} \geq m_i; \end{aligned} \tag{2}$$

By scanning the number of h_c signal events in the fit to the $\gamma\eta_c$ invariant mass spectrum, the likelihood value as a function of expected signal events $\mu_i^{\rm sig}$ is obtained. The parameters of the Gaussian function are determined from a fit to the likelihood distribution. For the R-scan data sample, the likelihood is defined as:

$$L_j(\mu_j^{\rm sig}; N_j^{\rm sig}, N_j^{\rm side}) = \int_0^\infty P(N_j^{\rm sig}; \mu_j^{\rm sig} + f \cdot \mu_j^{\rm bkg}) P(N_j^{\rm side}; \mu_j^{\rm bkg}) d\mu_j^{\rm bkg}, \tag{3}$$

where $P(N; \mu) = \frac{1}{N!}\mu^N e^{-\mu}$ is the Poisson distribution, $\mu_j^{\rm sig}$ and $\mu_j^{\rm bkg}$ are the number of expected number of signal and background events, respectively.

Correlation matrix from the fit to the cross section

The correlation matrix of the fit parameters from the fit the to the dressed cross sections of $e^+e^- \to \pi^+\pi^- h_c$ is

$$\begin{array}{c} \\ M_1 \\ \Gamma_1 \\ (\Gamma_{ee}\mathcal{B})_1 \\ \phi \\ M_2 \\ \Gamma_2 \\ (\Gamma_{ee}\mathcal{B})_2 \end{array} \begin{array}{c} \begin{array}{ccccccc} M_1 & \Gamma_1 & (\Gamma_{ee}\mathcal{B})_1 & \phi & M_2 & \Gamma_2 & (\Gamma_{ee}\mathcal{B})_2 \end{array} \\ \begin{pmatrix} 1.000 & -0.420 & 0.104 & 0.136 & 0.184 & -0.449 & 0.078 \\ & 1.000 & 0.191 & 0.077 & 0.478 & 0.096 & 0.079 \\ & & 1.000 & 0.992 & 0.020 & -0.102 & 0.985 \\ & & & 1.000 & -0.049 & -0.119 & 0.993 \\ & & & & 1.000 & -0.306 & -0.113 \\ & & & & & 1.000 & -0.017 \\ & & & & & & 1.000 \end{pmatrix} \end{array}$$

where M_j, Γ_j, and $(\Gamma_{ee}\mathcal{B})_j$ $(j = 1,\ 2)$ are the mass, the total width, and the product of the electronic partial and the branching fraction to $\pi^+\pi^- h_c$ for the two resonances, respectively; ϕ is the relative phase between two Breit-Wigner functions.